Available online at www.sciencedirect.com

ScienceDirect

Acta Materialia 84 (2015) 164–171

Acta MATERIALIA

www.elsevier.com/locate/actamat

# Local structure and hybridization states in $Ba_{0.9}Ca_{0.1}Ti_{1-x}Zr_xO_3$ ceramic compounds: Correlation with a normal or relaxor ferroelectric character

V.R. Mastelaro,[a,*] H.R. Favarim,[b] A. Mesquita,[c] A. Michalowicz,[d] J. Moscovici[d] and J.A. Eiras[e]

[a] *Instituto de Física de São Carlos, Universidade de São Paulo, São Carlos, SP, Brazil*
[b] *DEFIS – Universidade Federal de Ouro Preto, Ouro Preto, MG, Brazil*
[c] *Departamento de Física, Instituto de Geociências e Ciências Exatas, Universidade Estadual Paulista, Rio Claro, SP, Brazil*
[d] *Institut de Chimie et des Materiaux Paris Est, CNRS and Université Paris Est Créteil, 94320 Thiais, France*
[e] *Departamento de Física, Universidade Federal de São Carlos, São Carlos, SP, Brazil*

Received 1 April 2014; revised 22 September 2014; accepted 27 October 2014
Available online 25 November 2014

**Abstract**—This paper reports on a multi-edge X-ray absorption analysis to elucidate how the substitution of $Ti^{4+}$ by $Zr^{4+}$ ions acts on the local order structure and on the O 2*p* hybridization states of $Ba_{0.9}Ca_{0.1}Ti_{1-x}Zr_xO_3$ (BCZT) lead-free ceramic compounds, inducing a ferroelectric evolution from a normal to a relaxor character. Ti, Ba, Zr and O X-ray absorption spectra were measured to probe the local and electronic structure of BCZT samples that exhibit a normal ($x < 0.18$) or relaxor ($x \geqslant 0.18$) ferroelectric character. X-ray absorption near edge structure results show that the local symmetry and distortion of $TiO_6$, $ZrO_6$ and $BaO_{12}$ units are not significantly affected by the Ti/Zr ratio, the ferroelectric character or the long-range order symmetry. The assignment of the ab initio density of states associated with the O K-edge enabled a correlation between the decrease in the hybridization between O 2*p* and Ti 3*d* states and the ferroelectric character evolution of the BCZT samples. The hybridization states in the ferroelectric relaxor samples exhibit a more symmetric spatial configuration, as occurs with long-range symmetry.


*Keywords:* Ferroelectrics; Relaxors; Lead-free; Hybridization; XAS

## 1. Introduction

Because of their wide range of applications with regard to high-performance materials and their exceptional dielectric, electromechanical and pyroelectric properties, relaxor ferroelectric compounds have been studied in much detail [1–4]. However, the relaxation mechanisms underlying their unique dielectric behavior are still far from well understood, and this is an obstacle for the further development and optimization of their desirable dielectric properties, such as high dielectric constant, low dielectric loss and high field tunability [1–7].

Compositional disorder, i.e. the disorder in the arrangement of different ions on crystallographically equivalent sites, has been pointed out as being a common feature of relaxors [1–7]. The relaxor behavior was first observed in perovskites with disorder in non-isovalent ions, including stoichiometric complex compounds, e.g. $Pb(Mg_{1/3}Nb_{2/3})O_3$ and $Pb(Sc_{1/2}Ta_{1/2})O_3$ (in which $Mg^{2+}$, $Sc^{3+}$, $Ta^{5+}$ and $Nb^{5+}$ ions are fully or partially disordered in the B-sublattice of the perovskite $ABO_3$ structure) and nonstoichiometric solid solutions, e.g. $Pb_{1-3x/2}La_xZr_{1-y}Ti_yO_3$ (PLZT), where the substitution of $Pb^{2+}$ by $La^{3+}$ ions necessarily leads to vacancies on the A-site [1–7].

Ceramic samples based on barium titanate ($BaTiO_3$ – BT) are among the most studied lead-free ferroelectric materials. The ferroelectric nature and the structural and dielectric phase transition temperatures of BT have been significantly investigated via a partial substitution of either Ba ions (A-site substitution) and/or Ti ions (B-site substitution) [8–13].

If a heterovalent atom substitutes for the Ba atom, a relaxor state is induced at lower amounts of Ti substitution [8–13]. In this case, as proposed for lead-containing relaxors, the relaxor state should be developed either by charge disorder or A-site vacancy [6]. On the other hand, in the substitution of $Ti^{4+}$ by $Zr^{4+}$ ions, which exhibit only a small difference in their ionic radii, the mechanism involved in the formation of polar nanoregions in $BaTiO_3$-based relaxors has not been elucidated.

A few studies have revealed that the polar behavior of BT-based relaxors is substantially related to displacements of $Ti^{4+}$ ions from the central position in the oxygen octahedra [6,13]. Indeed, the relaxor state in the $BaZr_xTi_{1-x}O_3$ (BZT) system, when $x \geqslant 0.25$, has been attributed to a breakage in the correlation displacement of B-site cations

* Corresponding author. Tel.: +55 16 33739828; fax: +55 16 33739824; e-mail: valmor@ifsc.usp.br

http://dx.doi.org/10.1016/j.actamat.2014.10.059
1359-6462/

caused by the substitution of $Ti^{4+}$ by $Zr^{4+}$, which hinders the perfect alignment of all Ti displacements [6,14,15].

As such remarkable materials are invariably chemically and/or displacively disordered, the study of their local and electronic structures is an important starting point to better understand their intrinsic dielectric properties.

Laulhé et al. [14] studied the short-range order structure around Zr atoms in the BZT system. According to their results, the local structure around Zr differs considerably from the average cubic structure determined by X-ray diffraction (XRD) and the distance between Zr atoms and their first oxygen neighbors is equal to the distance measured in the $BaZrO_3$ compound independently of the Zr substitution rate. The authors observed that Zr atoms tended to be segregated in Zr-rich regions and the relaxor behavior in BZT could be influenced by the random elastic fields generated by the chemical arrangement of Zr atoms.

The analysis of the neutron pair distribution function was also used for the study of the local structure in BZT relaxors [15]. Despite the Ti/Zr substitution and their different dielectric properties, Ti displacements in BZT relaxors are similar to those in the classical BT compound. Laulhé et al. [15] concluded that the difference in the dielectric properties of BT and BZT materials lies in the different correlation between the cations displacements.

Laulhé et al. [16] also proposed an explanation for the relaxor behavior of the $BaTi_{0.74}Zr_{0.26}O_3$ sample using first-principles supercell calculations. Based on the calculations, they asserted that the symmetry of a Ti atom displacement is fully determined by the distribution of the Ti and Zr atoms in the adjacent unit cells. Unlike what is observed in the classic BT compound, in the $BaTi_{0.74}Zr_{0.26}O_3$ relaxor, the chemical substitution imposes a random distribution of the Ti displacement symmetries between the $TiO_6$ octahedra, thereby inhibiting the perfect alignment of all Ti displacements. This degree of freedom would lead to a partial correlation of the polar displacement, hence the formation of polar nanoregions [16].

Knowledge of the electronic and local structures of ferroelectric ceramics is a fundamental step towards understanding their dielectric properties. In lead-based ferroelectric ceramic systems, the ferroelectric character is directly correlated with the electronic properties of both A-site ($Pb^{2+}$) and B-site ($Ti^{4+}$) ions [17,18]. Many studies have shown that the density of states (DOS) of oxygen and titanium atoms could provide a more direct correlation with the ferroelectric stability of perovskite-based compounds [19–28]. They have also reported a significant modification in the hybridization among O 2*p*, Pb 6*sp* and Ti 3*d* states when the ferroelectric character changes.

In the PLZT and $Pb_{1-x}Ba_xZr_{1-y}Ti_yO_3$ complex ferroelectric compounds, a reduction in the degree of hybridization between O 2*p* and Pb 6*sp* (Ti 3*d*) states as the amount of La (Ba) increased was directly related to the manifestation of the relaxor character [23–28].

To the best of our knowledge, no investigation into the evolution from a normal character to a relaxor one and the hybridization state of the ions has been conducted in lead-free systems. Thus, this paper presents a multi-edge X-ray absorption spectroscopy (XAS) analysis to investigate how the substitution of $Ti^{4+}$ by $Zr^{4+}$ ions acts on the local structure and hybridization states of $Ba_{0.9}Ca_{0.1}Zr_xTi_{1-x}O_3$ (BCZT) lead-free ceramic compounds and how the results could be related to their ferroelectric character. The local and electronic structures of BCZT ceramic samples prepared by the solid-state reaction procedure were studied by measuring the XAS spectra at the Ti K- and L-edges and the Zr, Ba and O K-edges. Since the Ba L-edge is just above the Ti K-edge, the latter was studied only by the X-ray absorption near edge structure (XANES). On the other hand, precise extended X-ray absorption fine structure (*EXAFS*) fitting procedures were used to determine the local structure around Ba and Zr atoms. Furthermore, we applied an ab initio method using the FEFF code [29] to interpret the O K-edge XANES signal of the two most representative BCZT samples in terms of hybridization states.

## 2. Experimental details

$Ba_{0,9}Ca_{0,1}Ti_{1-x}Zr_xO_3$ ceramic samples, hereafter labeled BCZT100*$x$ (where $x = 0.00$, 0.05, 0.09, 0.18, 0.20, 0.22, 0.24 and 0.27), were prepared by the solid-state reaction method. A detailed description of the sample preparation can be found elsewhere [30].

Titanium K-edge X-ray absorption spectra were collected at the LNLS (National Synchrotron Light Laboratory) facility using the D04B-XAS2 beamline. The sample pellets, obtained after sintering, were ground and XAS data were measured in transmission mode from 80 to 430 K using a double crystal Si(1 1 1) monochromator. Ionization chambers were used to detect the incident and transmitted flux. XANES spectra at the Ti K-edge were recorded for each sample between 4910 and 5200 eV using energy steps of 0.5 eV around the edge. For good energy reproducibility during the XANES data collection, the energy calibration of the monochromator was checked with a Ti metal foil at the same time as the sample spectra were collected. Titanium L-edges and oxygen K-edge XANES spectra were measured by the electron yield mode using the SGM beamline at the Canadian Light Source synchrotron facility. The Zr and Ba K-edge EXAFS spectra were collected at the SOLEIL Synchrotron facility using SAMBA beamline with a Si (2 2 0) sagittal focusing monochromator.

The XANES normalization and the extraction of EXAFS spectra were performed using the Multi-Platform Applications for X-ray absorption (MAX) software package [31]. Normalized XANES and EXAFS fitting were obtained with the MAX-Cherokee and MAX-Roundmidnight codes, respectively. The amplitude and phase shift data were calculated using the FEFF8 theoretical ab initio code with the input files issued from MAX-Crystalffrev [29,32]. The MAX-Crystalffrev code enables substitutions and vacancies in the input crystal structure obtained from Rietveld refinements [30]. EXAFS data fitting used the standard EXAFS formula according to the reports of the IXS standard and criteria subcommittees [33].

FEFF9 ab initio real-space code was used to model the O K-edge XANES spectra and determine the oxygen DOS of BCZT00 and BCZT27 samples [34]. The code employs full multiple scattering and the muffin-tin approximation for wave function expansion to determine a periodic potential and calculate the absorption spectrum for the scattering atom. XANES FEFF spectra were calculated using a self-consistent field approximation within a 12 Å radius from the central O atom. The partial DOS spectra were calculated for the absorbing oxygen atom and all neighboring atoms (O, Ti, Zr, Ca and Ba) were considered.

## 3. Results and discussion

Table 1 shows a summary of previously obtained XRD refinements and the dielectric response of BCZT samples [29]. As can be seen, the long-range order changes from tetragonal (BCZT00) to cubic (BCZT05 to BCZT27) symmetry, while the dielectric response moves from a ferroelectric to a relaxor character.

### 3.1. Ti K-edge XANES spectra analysis

Fig. 1 shows the Ti K-edge XANES spectra of the BCZT samples. No significant variation was observed in the spectra as the amount of Zr increased, indicating that the local order structure around titanium atoms did not undergo any significant change as Ti atoms were replaced by Zr atoms.

According to the experimental and theoretical study of Vedrinskii et al. [35], in most $ABO_3$ centrosymmetric perovskite compounds, such as $EuTiO_3$, $SrTiO_3$ and $CaTiO_3$, three pre-edge peaks, labeled *A*, *B* and *C*, are observed at the Ti K-edge XANES spectra. In all ferroelectric titanate perovskites with a distorted $TiO_6$ octahedral site, the quadripolar *1s*–3*d* transition labeled *A* is almost totally hidden by the quite intense peak *B* [35]. The authors proved that the dipolar *1s*–3*d* ($t_{2g}$) transition labeled *B* is related to the hybridization of *p*- and *d*-symmetric states of Ti atom under the influence of the neighboring oxygen atoms [35]. For perovskites, the off-center displacement (static and/or dynamic) of the Ti atom in the $TiO_6$ octahedron can be related to the area under the B peak in the *1s*–3*d* transition region [35–37]. As can be observed in Fig. 1b, the *B* peak areas of BCZT00 and BCZT27, characterized as normal and relaxor ferroelectric samples, respectively, are similar to that of the $BaTiO_3$ (BT) ferroelectric phase. According to Ravel et al. [38], independently of the BT crystallographic symmetry, the distortion of Ti atoms calculated from the analysis of the B peak area is around 0.18.

The pre-edge feature labeled *C* is related to the Ti *1s* electron transition to the unoccupied 3*d*-originated $e_g$-type molecular orbital of the $TiO_6$ polyhedra neighboring the absorbing Ti atoms [35–37]. The $t_{2g}$–$e_g$ energy gap between peaks *B* and *C* is approximately 3 eV (24,200 $cm^{-1}$), which is in the expected range for $TiO_6$ octahedral sites. The area under peak *C* does not depend strongly on small displacements of the atoms from their sites, but it changes significantly when 4*d* atoms appear in the vicinity of the absorbing Ti atom [35]. Fig. 1c shows that the peak C intensity varies as the amount of Zr increases, confirming the substitution of Ti nearest neighbors by Zr atoms.

**Table 1.** Space groups and cell parameter obtained from Rietveld refinement of BCZT ceramics and their dielectric response at room temperature [30].

| Sample | Space group | *a* (Å) | Dielectric response |
|---|---|---|---|
| BCZT00 | P4mm | 3.99862 | Ferroelectric |
| BCZT05 | Pm-3m | 4.01154 | Ferroelectric |
| BCZT09 | Pm-3m | 4.02101 | Paraelectric |
| BCZT18 | Pm-3m | 4.04207 | Relaxor |
| BCZT20 | Pm-3m | 4.04119 | Relaxor |
| BCZT22 | Pm-3m | 4.04903 | Relaxor |
| BCZT24 | Pm-3m | 4.05199 | Relaxor |
| BCZT27 | Pm-3m | 4.05746 | Relaxor |

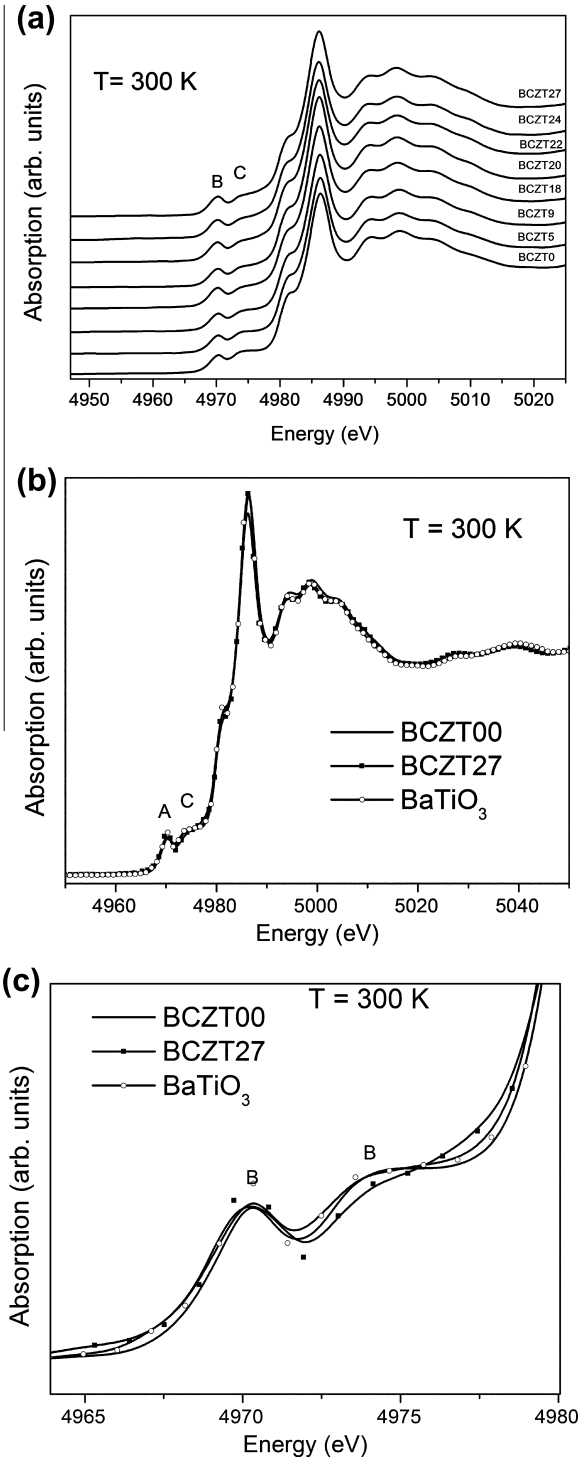


**Fig. 1.** (a) Ti K-edge XANES spectra of BCZT samples collected at room temperature, (b) XANES spectra of BCZT00, BCZT27 and $BaTiO_3$ samples measured at 300 K and (c) details of the pre-edge region peaks of (b).

In summary, the results obtained at the Ti K-edge XANES spectra show that, independently of the long-range order symmetry and ferroelectric character, Ti atoms are located in an off-center position and their degree of disorder is similar to that observed in the $BaTiO_3$ compound.

### 3.2. Zr K-edge EXAFS data analysis

Fig. 2 shows the Zr K-edge EXAFS spectra and the respective Fourier transform (FT) curves of the $BaZrO_3$, BCZT09 and BCZT27 samples. The first FT peak of the BCZT samples, which corresponds to the Zr–O distance, shows a shorter distance in comparison to that in the $BaZrO_3$ compound and its intensity decreases as the amount of Zr increases. The second shell corresponds to Zr–Ba(Ca), Zr–Ti(Zr) and Zr–Zr, as well as contributions from multiple scattering effects. Theoretical calculations issued from FEFF code (not showed) indicate that the significant modification in the intensity of the second shell as the amount of Zr increases is due to the difference in the backscattering phases of Ti and Zr atoms. Thus, only the first Zr–O coordination shell is analyzed quantitatively because it is more directly correlated to the $TiO_6$ octahedra and the evolution from a normal to a relaxor ferroelectric character.

Table 2 shows the fitting results of Zr K-edge EXAFS spectra that correspond to the first coordination shell (Zr–O) and Fig. 3 shows a comparison between the filtered and theoretical EXAFS spectra of the BCZT27 sample. As can be observed, the Zr–O mean bond lengths of BCZT samples are similar, whereas the Debye–Waller factor value increases as Ti is substituted by Zr atoms. Such results are similar to those obtained by Laullhé et al. in the analysis of the local order structure around Zr atoms in the $BaTi_{1-x}Zr_xO_3$ samples [15]. As also stated by the authors, in BZT samples, the structural differences observed around Zr atoms between the BCZT09 and BCZT27 samples are too small to explain the modification in their ferroelectric character.

### 3.3. Ba K-edge EXAFS data analysis

Fig. 4 shows the Ba K-edge EXAFS spectra and FT curves of the BCZT09, BCZT18, BCZT24 and BCZT27 samples. As the amount of Zr increases, the intensity of the FT peaks decreases and the peak positions are not significantly affected. The decrease in the intensity of the FT peaks can be interpreted in terms of either a decrease in the number of Ba neighbors or an increase in the Debye–Waller factor value. According to previous XRD studies [30], these samples exhibit a cubic symmetry at room temperature. Therefore, at least for the Ba–O first coordination shell, no variation in the number of neighbors is expected.

In order to identify the origin of the FT intensity decrease, the peaks between 1.5 and 4 Å were isolated and back-Fourier transformed, and the filtered EXAFS

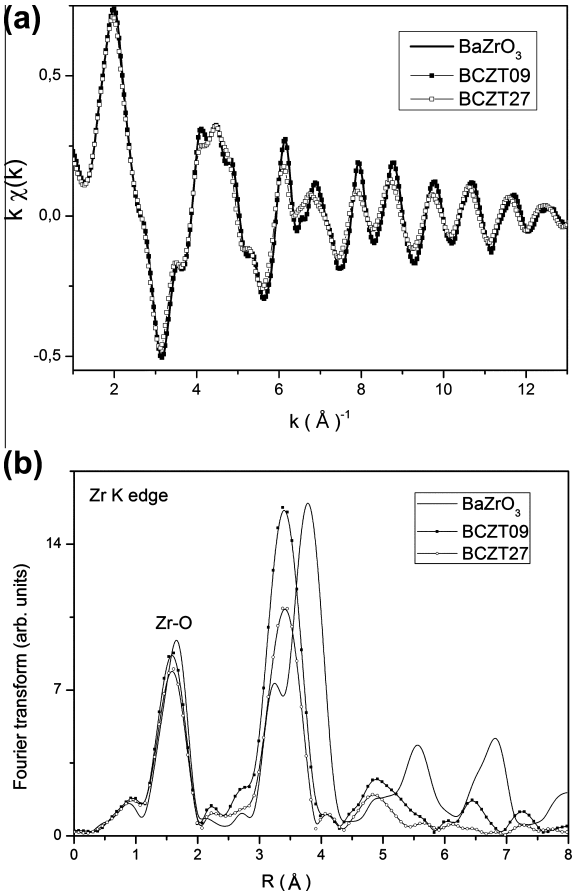


**Fig. 2.** (a) Zr K-edge EXAFS spectra and (b) FT of BZ and BCZT samples collected at 300 K.

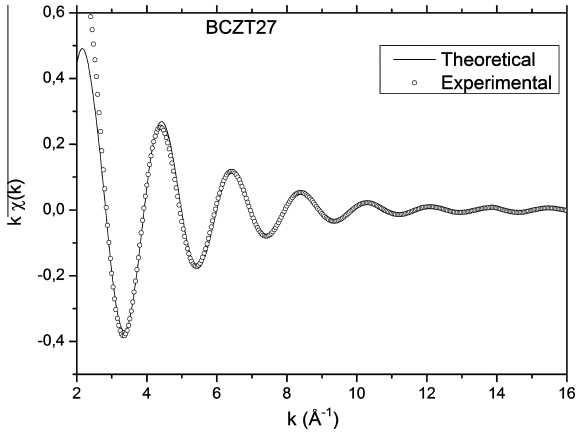


**Fig. 3.** Comparison between filtered EXAFS spectra (dots) and theoretical EXAFS spectra (line) of the BCZT27 sample.

**Table 2.** Fitting results of the first coordination shell of EXAFS spectra collected at the Zr K-edge at 300 K and the Zr–O mean bond-length obtained from XRD.

| Sample | N (Zr–O)* | R (Zr–O) Å | $\sigma^2$ (Zr–O) Å | QF | R (Zr–O) Å XRD |
|---|---|---|---|---|---|
| $BaZrO_3$ | 6 | 2.113 ± 0.004 | 0.0047 ± 0.0003 | 1.1 | 2.10 |
| BCZT09 | 6 | 2.109 ± 0.005 | 0.0056 ± 0.0004 | 1.8 | 2.11 |
| BCZT27 | 6 | 2.103 ± 0.005 | 0.0065 ± 0.0004 | 1.7 | 2.11 |

QF = quality factor.
* Fixed during the fitting procedure.

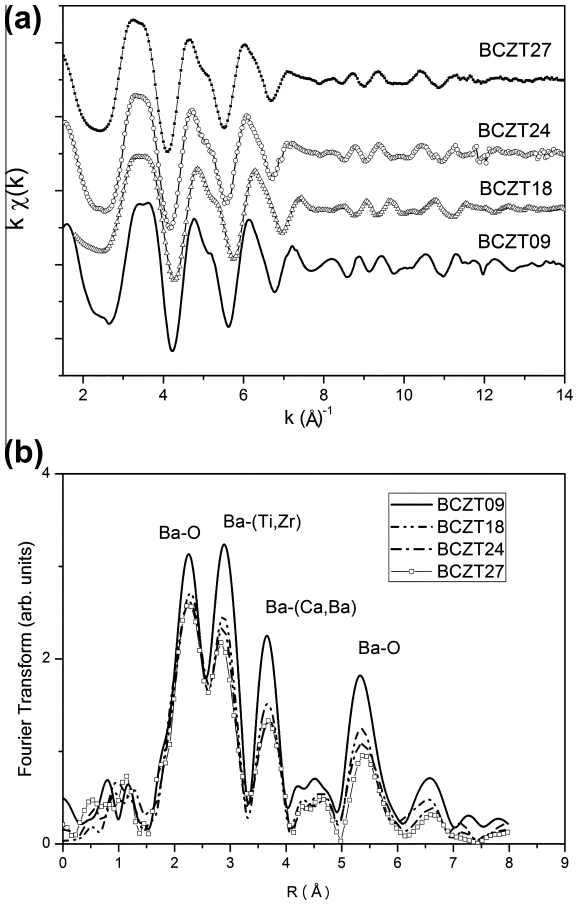


**Fig. 4.** (a) Ba K-edge EXAFS spectra and (b) respective FT of BCZT samples collected at room temperature.

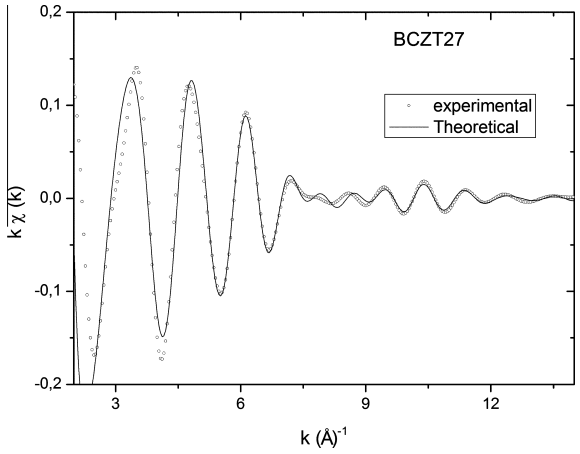


**Fig. 5.** Comparison between filtered EXAFS spectra (dots) and theoretical EXAFS spectra (line) of the BCZT27 sample.

spectra were fitted. Table 3 shows the fitting results of the first three FT peaks, which correspond, respectively, to Ba–O, Ba–(Ti,Zr) and Ba–(Ba,Ca) interactions. Fig. 5 shows the comparison between the filtered EXAFS spectra of the BCZT27 sample and the theoretical EXAFS spectra obtained after the fitting procedure. The amounts of Zr and Ca were taken into account by considering the nominal sample composition, and the neighbor's numbers of each shell was fixed during the fitting procedure. A better quality factor was attained when the Ba–Zr, Ba–Ti, Ba–Ca and Ba–Ba contributions were considered separately. According to the fitting results, the first Ba–O bond length increased from 2.82 to 2.85 Å as the amount of Zr increased. Concerning the Ba–Ti, Ba–Zr and Ba–(Ba,Ca) interactions, the bond lengths also increased and the Debye–Waller factor ($\sigma$) values remained practically constant as the amount of Zr increased. Therefore, the decrease in the intensity of the FT peaks with increasing amount of Zr cannot be attributed to the increase in the disorder around the Ba atoms. In fact, FEFF theoretical calculations show a phase opposition between Ti and Zr signals that could explain the intensity decrease as Ti is substituted by Zr atoms: a variation in the Ti/Zr number of neighbors, even with small distance variations, can lead to a significant interference effect on the EXAFS signal. Due to the superposition of the three FT peaks, this phase opposition effect also affects the amplitude of the Ba–O interaction.

The results of barium EXAFS spectra show that the short-range order structure around Ba atoms is not significantly affected by the modification in the long-range order structure of the ferroelectric phase. Moreover, as can be observed in Fig. 6, the structural results from the analysis of the Ba EXAFS spectra showed a good agreement with those from the XRD analysis [30].

### 3.4. Ti L-edge and O K-edge XANES data analysis

The Ti L-edge XANES spectra of $BaTiO_3$ and BCZT samples (Fig. 7) show two pre-edge peaks, denoted as *A* and *B,* and a usual set of four peaks, denoted as *C*, *D*, *E* and *F*. As can be observed, increasing the amount of Zr promotes no significant changes in the spectra. The Ti L-edge XANES spectra of the $BaTiO_3$ compound have been studied in detail previously [19–22]. According to these

**Table 3.** Fitting results of the first three coordination shells of BCZT EXAFS spectra at Ba K-edge collected at 300 K.

| Sample $x$ | $N^*_{Ba-O}$ | $R_{Ba-O}$ | $\sigma_{Ba-O}$ | $N^*_{Ba-Ti}$ | $R_{Ba-Ti}$ | $\sigma_{Ba-Ti}$ | $N^*_{Ba-Zr}$ | $R_{Ba-Zr}$ | $\sigma_{Ba-Zr}$ | $N^*_{Ba-(Ba,Ca)}$ | $R_{Ba-(Ba,Ca)}$ | $\sigma_{Ba-(Ba,Ca)}$ | QF |
|---|---|---|---|---|---|---|---|---|---|---|---|---|---|
| 0.09 | 12 | 2.820 | 0.0133 | 7.0 | 3.480 | 0.0086 | 1.0 | 3.55 | 0.0045 | 6.0 | 4.014 | 0.0096 | 4.3 |
| | | (0.009) | (0.0008) | | (0.006) | (0.0007) | | (0.01) | (0.0008) | | (0.006) | (0.003) | |
| 0.18 | 12 | 2.837 | 0.0145 | 7.0 | 3.492 | 0.0075 | 1.0 | 3.53 | 0.0065 | 6.0 | 4.030 | 0.012 | 3.1 |
| | | (0.009) | (0.009) | | (0.007) | (0.0007) | | (0.01) | (0.0007) | | (0.009) | (0.001) | |
| 0.22 | 12 | 2.850 | 0.0144 | 6.0 | 3.520 | 0.009 | 2.0 | 3.550 | 0.0059 | 6.0 | 4.05 | 0.014 | 2.0 |
| | | (0.009) | (0.0009) | | (0.008) | (0.001) | | (0.009) | (0.0007) | | (0.01) | (0.001) | |
| 0.27 | 12 | 2.850 | 0.0147 | 5.0 | 3.52 | 0.0083 | 3.0 | 3.55 | 0.0075 | 6.0 | 4.05 | 0.014 | 2.3 |
| | | (0.01) | (0.0009) | | (0.01) | (0.0009) | | (0.01) | (0.0006) | | (0.01) | (0.001) | |

() error; $N_{Ba-Ti} + N_{Ba-Zr} = 8$, $N_{Ba-Ba} + N_{Ba-Ca} = 6$, QF = quality factor.
* Fixed during the fitting procedure.

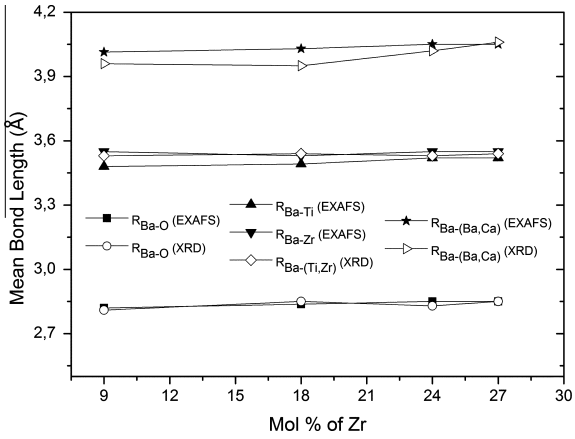


**Fig. 6.** Comparison of Ba–O, Ba–Ti, Ba–Zr and Ba–(Ba,Ca) mean bond lengths determined from EXAFS fitting and obtained from the XRD refinement provided in Ref. [30].

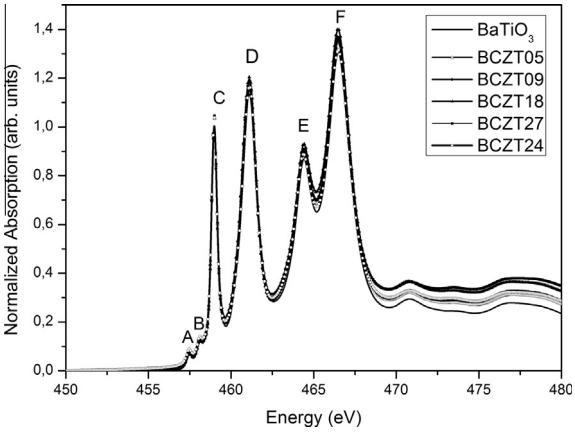


**Fig. 7.** Titanium L-edge XANES spectra of $BaTiO_3$ and BCZT compounds collected at 300 K.

studies, the features labeled *A* and *B* are related to forbidden dipolar transitions in the L–S coupling (spin–orbit coupling) allowed by *pd* multipolar interactions [19–22]. Features *C* and *D* occur because the 3*d* band splits into two sub-bands in the Ti $L_{III}$-edge, i.e. $t_{2g}$ (peak *C*) and $e_g$ (peak *D*) [19–22]. The other two features, *E* and *F*, correspond to the $L_{II}$-edge with $t_{2g}$ and $e_g$ symmetries, respectively. In good agreement with the analysis of the Ti K-edge data, all Ti L-edge XANES spectra of BCZT samples are similar to that of the $BaTiO_3$ compound and are not affected by the increase in the amount of Zr.

Fig. 8 shows the O K-edge XANES spectra of $BaTiO_3$ and BCZT compounds. As can be observed in Fig. 8a, increasing the amount of Zr promotes a systematic decrease in the *A* peak intensity. On the other hand, the changes in the *B* and *C* features are more complex, since they tend to overlap as the amount of Zr increases above $x = 0.09$. The *D* and *E* peaks remain quite stable as the amount of Zr increases. According to the literature, the features observed in O K-edge XANES spectra are due to transitions from the O 1*s* core state to the unoccupied O 2*p*-derived state [19–22]. More specifically, the features labeled *A*, *B* or *C* are attributable to hybridized states between O 2*p* and Ti 3*d*, whereas features *D* and *E* are attributable to the O 2*p*-derived states hybridized with Ca 3*d*/Ba 5*d* [19–21]. As

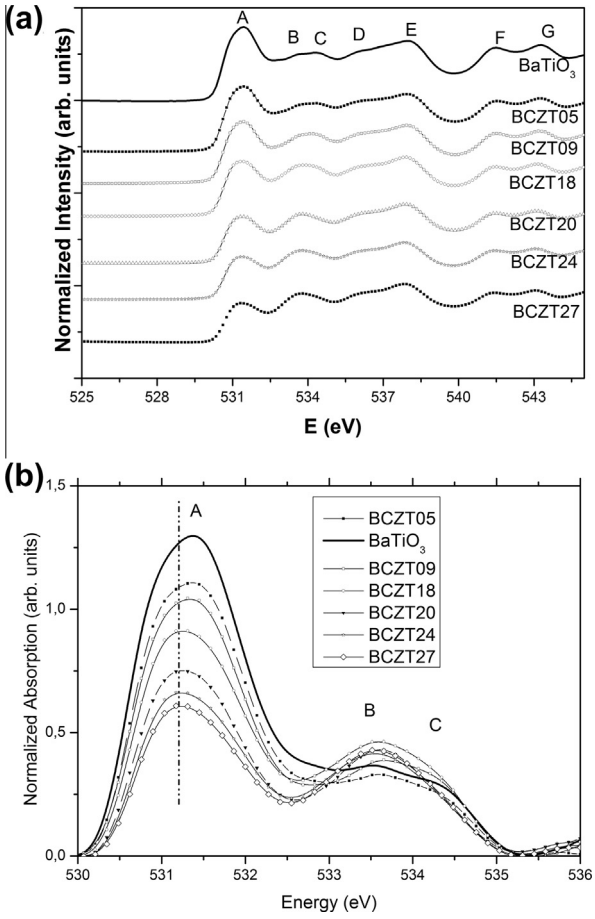


**Fig. 8.** (a) O K-edge XANES spectra of $BaTiO_3$ and BCZT samples. (b) Details of the edge region where the modifications are more significant.

the electronegativity of Zr (1.33) is lower than that of Ti (1.54), feature *A* shifts slightly to lower energy as the Zr content increases [20].

In order to correlate the modifications observed at the O K-edge spectra and the electronic structure of oxygen atoms, the O K-edge X-ray absorption spectra and the O 2*p*, Ti 3*d*, Zr 3*d*, Ca 3*d* and Ba 5*d*-derived density of states for two representative samples, BCZT00 (normal ferroelectric) and BCZT27 (relaxor ferroelectric), were calculated. The O K-edge theoretical XANES spectra and the DOS of the BCZT00 and BCZT27 samples were calculated using the FEFF9.0 code and considering an ensemble of atoms around the central oxygen atom [34]. These ensembles, which contain 540 atoms and correspond to a 10.14 Å cluster radius around the absorbing atom (oxygen), were constructed based on the average X-ray diffraction structure of both compounds previously determined [30]. The ground state DOS was calculated with the same code parameters. The total O XANES spectrum was obtained by summing the contributions of two individual O-atom sites and at least three XANES spectra calculated and averaged to take into account the different possible positions of the substituting atoms (Ca and Zr). The energy scale of the O 2*p*-projected DOS calculated by FEFF9.0 code was shifted so that the peak positions could be compared with the experimental XANES spectra. The partial DOS has been broadened with a Lorentzian function of 0.2 eV half-width at half maximum.

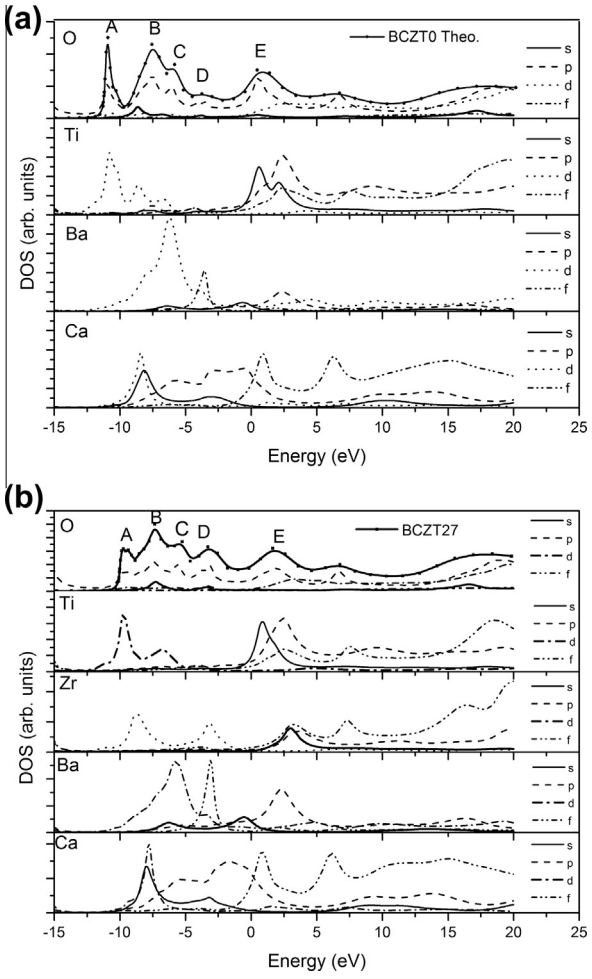


**Fig. 9.** O K-edge XANES spectra of: (a) the BCZT00 sample and (b) the BCZT27 sample, with their respective partial electron energy DOS.

Fig. 9 shows the calculated O K-edge XANES spectra of the BCZT00 and BCZT27 samples and the local density of states (*s*-, *p*-, *d*- and *f*-projected DOS) of oxygen, titanium, zirconium, barium and calcium. In both cases, the O 2*p*-projected DOS resembles the experimental O K-edge XANES spectra calculated. Moreover, from the position of the density of the states peaks, it was possible to infer that feature *A* results mainly from O 2*p* states hybridized with the Ti 3*d* orbital. Features *B* and *C* come up largely from the hybridization between the O 2*p* and the Ba *5d* and Ca 3*d* states. Feature *D* arises predominantly from the hybridization between the O 2*p* and the Ba 4*f* and Ca 2*p* states, whereas feature *E* can be assigned mainly to a hybridization of O 2*p* with Ti 2*p*4*f* and Ca 4*f*. Fig. 9 shows the intensity of the Ti 3*d*, Zr 4*d*, Ba 4*f* and Ca 3*d* DOS divided by a factor of 2, 5 or 10 so that the projected DOS can be compared on a common intensity scale.

Thus, the decrease in the feature *A* intensity and the evolution of the ferroelectric character observed experimentally in BCZT samples as the amount of Zr increased can be directly correlated to the hybridization decrease between the O 2*p* and Ti 3*d* states. Furthermore, as the amount of Ca and Ba atoms remained constant in the samples studied, the overlap of the *A* and *B* peaks can be attributed mainly to modifications to the degree of hybridization between the O 2*p* with Ti 3*d* states.

It is well accepted that the ferroelectric ordering results from a balance between the long-range Coulomb interaction and short-range forces [17]. As in other perovskites, the hybridization between Ti 3*d* and O 2*p* weakens the short-range repulsions in the BCZT samples and enables the establishment of a ferroelectric order [18,19]. The intensity drops of feature *A* with increasing Zr content indicate a decrease in the number of unoccupied O 2*p*–Ti 3*d* hybridized states. According to Cohen [17], if the Ti–O hybridization is inhibited, the ferroelectric instability disappears and the cubic phase is more stable. Based on these considerations, we propose that the reduction in the O 2*p*–Ti 3*d* hybridization caused by the substitution of Ti by Zr decreases the ferroelectric instability, favoring the relaxor character in samples with $x \geqslant 0.18$.

## 4. Conclusions

This paper has reported a comprehensive experimental analysis of the short-range order and electronic structure of $Ba_{0.9}Ca_{0.1}Zr_xTi_{1-x}O_3$ (BCZT) lead-free ferroelectric ceramic compounds. The local and electronic structure around all constituent Ba, Ti, O and Zr atoms were studied as a function of the substitution of Ti by Zr.

The XANES spectra of BCZT and $BaTiO_3$ samples collected at the Ti K- and L-edges showed that the local and electronic structures of Ti atoms are very similar and remain distorted, despite their different ferroelectric responses, especially in the case of relaxor samples which were assigned as cubic from XRD. From the Ti K-edge XANES spectra, no different displacement direction of Ti was identified, which indicates that no structural changes occur in the $TiO_6$ octahedra with increasing amount of Zr.

The fitting results of barium EXAFS spectra show that the short-range order structure around Ba atoms is in good agreement with that obtained from the XRD analysis and is not significantly affected by the modification in the long-range order structure or the ferroelectric state.

The structural variations observed around Zr atoms are too small to explain the modification in the ferroelectric character caused by the increase in the amount of Zr.

The calculation of the DOS of the constituent atoms in a normal and a relaxor BCZT sample showed that the intensity decrease observed at the O K-edge XANES spectra as the amount of Zr increases is directly correlated to a decrease in the hybridization between the O 2*p* and Ti 3*d* states. Such a result has led to the conclusion that this hybridization reduction favors the relaxor character above a certain amount of Zr.

The decrease in O 2*p* hybridization with Ti 3*d* is similar to that observed in lead-based ferroelectric ceramic materials, although in the BCZT samples the substitution occurs only on the B (Ti) site.

Although the local structure around the Ti atoms of the BCZT samples is similar to that observed in the $BaTiO_3$ compound, the hybridization states change to a more symmetric spatial configuration, as occurs with the long-range symmetry when Ti is substituted by Zr atoms.

## Acknowledgements

The authors are grateful to FAPESP (Proc.: 2008/04025-0) and Capes Brazilian funding agencies. This research was partially

carried out at the LNLS, SOLEIL and CLS synchrotron facilities. The storage ring operators and XAS beamline scientists of the three synchrotrons (S. Belin, V. Briois, E. Fonda (Soleil), A.P.S. Sotero and J.C. Maurício (LNLS) and T. Regier and D. Chevrier (CLS)) are highly acknowledged.

## References

[1] V.A. Isupov, Phys. Solid State 45 (2003) 1107.
[2] Z.G. Ye, Key Eng. Mater. 11 (1998) 81.
[3] A.A. Bokov, Z.G. Ye, J. Mater. Sci. 41 (2006) 31.
[4] R.A. Cowley, S.N. Gvasaliya, S.G. Lushnikov, B. Roessli, G.M. Rotaru, Adv. Phys. 60 (2011) 229.
[5] T. Maiti, R. Guo, A.S. Bhalla, Ferroelectrics 425 (2011) 4.
[6] V.V. Shvartsman, D.C. Lupascu, J. Am. Ceram. Soc. 95 (2012) 1.
[7] L. Xie, Y.L. Li, R. Yu, Z.Y. Cheng, X.Y. Wei, X. Yao, C.L. Jia, K. Urban, A.A. Bokov, Z.-G. Ye, J. Zhu, Phys. Rev. B 85 (2012) 014118.
[8] J. Ravez, C. Broustera, A. Simon, J. Mater. Chem. 9 (1999) 1609.
[9] J. Ravez, A. Simon, Eur. Phys. J. AP 11 (2000) 9.
[10] J. Ravez, A. Simon, J. Solid State Chem. 162 (2001) 260.
[11] A. Simon, J. Ravez, M. Maglione, Solid State Sci. 7 (2005) 925.
[12] J. Ravez, A. Simon, Eur. J. Solid State Inorg. Chem. 34 (1997) 1199.
[13] A. Simon, J. Ravez, M. Maglione, J. Phys. Condens. Matter 16 (2004) 963.
[14] C. Laulhé, F. Hippert, J. Kreisel, M. Maglione, A. Simon, J.-L. Hazemann, V. Nassif, Phys. Rev. B 74 (2006) 014106.
[15] C. Laulhé, F. Hippert, R. Bellissent, A. Simon, G.J. Cuello, Phys. Rev. B 79 (2009) 064104.
[16] C. Laulhé, A. Pasturel, F. Hippert, J. Kreisel, Phys. Rev. B 82 (2010) 132102.
[17] R.E. Cohen, Nature 358 (1992) 136–138.
[18] H. Miyazawa, E. Natori, S. Miyashita, T. Shimoda, F. Ishii, T. Oguchi, Jpn. J. Appl. Phys. 39 (Part 1) (2000) 5679.
[19] J.C. Jan, K.P.K. Kumar, J.W. Chiou, H.M. Tsai, H.L. Shih, H.C. Hsueh, S.C. Ray, K. Asokan, W.F. Pong, M.H. Tsai, S.Y. Kuo, W.F. Hsieh, Appl. Phys. Lett. 83 (2003) 3311.
[20] J.C. Jan, H.M. Tsai, C.W. Pao, J.W. Chiou, C.K. Asokan, K.P.K. Kumar, W.F. Pong, Y.H. Tang, M.H. Tsai, S.Y. Kuo, W.F. Hsieh, Appl. Phys. Lett. 87 (2005) 012103.
[21] P. Nachimuthu, S. Thevuthasan, E.M. Adams, W.J. Weber, B.D. Begg, B.S. Mun, D.K. Shuh, D.W. Lindle, E.M. Gullikson, R.C.C. Perera, J. Phys. Chem. B 109 (2005) 1337.
[22] S.O. Kucheyev, T.v. Buuren, T.F. Baumann, J.J.H. Satcher, T.M. Willey, R.W. Meulenberg, T.E. Felter, J.F. Poco, S.A. Gammon, L.J. Terminello, Phys. Rev. B 69 (2004) 245102.
[23] V.R. Mastelaro, P.P. Neves, S.R. de Lazaro, E. Longo, A. Michalowicz, J.A. Eiras, J. Appl. Phys. 99 (2006) 044104.
[24] V.R. Mastelaro, P.P. Neves, A. Michalowicz, J.A. Eiras, J. Phys. Condens. Matter 19 (2007).
[25] A. Mesquita, A. Michalowicz, V.R. Mastelaro, in: 14th international conference on X-Ray absorption fine structure (XAFS14), Proceedings book series: journal of physics conference series, vol. 190, 2009, p. 012081.
[26] V.R. Mastelaro, A. Mesquita, P.P. Neves, A. Michalowicz, M. Bounif, P.S. Pizani, M.R. Joya, J.A. Eiras, J. Appl. Phys. 105 (2009) 033508.
[27] V.R. Mastelaro, Y.P. Mascarenhas, P.P. Neves, M. Mir, A.C. Doriguetto, A. Michalowicz, J. Moscovici, M.H. Lente, J.A. Eiras, et al., J. Appl. Phys. 107 (2010) 114103.
[28] A. Mesquita, A. Michalowicz, V.R. Mastelaro, J. Appl. Phys. 111 (2012) 104110.
[29] A.L. Ankudinov, B. Ravel, S.D. Conradson, J.J. Rehr, Phys. Rev. B 58 (1998) 7565.
[30] H.R. Favarim, A. Michalowicz, J.C. M'Peko, V.R. Mastelaro, Phys. Status Solidi A 207 (2010) 2570.
[31] A. Michalowicz, J. Moscovici, D. Muller-Bouvet, K. Provost, J. Phys. Conf. Ser. 190 (2009) 012034.
[32] A. Michalowicz, J. Moscovici, D. Muller-Bouvet, K. Provost, J. Phys. Conf. Ser. 430 (2013) 012016.
[33] IXS Standards and Criteria Subcommittee Reports, International XAFS Society, <http://ixs.iit.edu/subcommittee_reports/sc/>, 2000.
[34] J.J. Rehr, J.J. Kas, F.D. Vila, M.P. Prange, K. Jorissen, Phys. Chem. Chem. Phys. 12 (2010) 5503.
[35] R.V. Vedrinskii, V.L. Kraizman, A.A. Novakovich, P.V. Demekhin, S.V. Urazhdin, J. Phys. Condens. Matter 10 (1998) 9561.
[36] A.I. Frenkel, D.M. Pease, J. Giniewicz, E.A. Stern, D.L. Brewe, M. Daniel, J. Budnick, Phys. Rev. B 70 (2004) 014106.
[37] V.L. Kraizman, A.A. Novakovich, R.V. Vedrinskii, V.A. Timoshevskii, Phys. B Condens. Matter 208 (1995) 35.
[38] B. Ravel, E.A. Stern, R.I. Vedrinskii, V. Kraizman, Ferroelectrics 206 (1998) 407.